Resilient Batch-Fabricated Planar Arrays of Miniaturized Langmuir Probes for Real-Time Measurement of Plasma Potential Fluctuations in the HF to Microwave Frequency Range

Emmanuel F. C. Chimamkpam, Ella S. Field, Akintunde Ibitayo (Tayo) Akinwande, *Fellow, IEEE*, and Luis Fernando Velásquez-García, *Senior Member, IEEE*

***Abstract*— We report the design, fabrication, and characterization of miniaturized, flush-mounted Langmuir probe arrays for RF diagnosis of plasmas in the HF to microwave range of frequencies. We developed probes of radii $\geq$125 μm by electroless nickel metallization of ultrasonically drilled through-substrate vias. Planar arrays with as many as 25 probes spaced 1.6 mm apart (39 probes/cm^2) in Pyrex, silicon carbide, and alumina substrates were produced. The sensor system was built to have a frequency response between 2 MHz and 3 GHz, and a probe impedance greater than or within close range of the plasma sheath impedance for plasma densities $\geq 10^{16}$ m^{-3}. We characterized a self-biasing nickel probe part of a 2 × 2 array with alumina substrate using a high-density magnetized helicon plasma source; we found that the measurement of the plasma potential from the MEMS probe compares well with independent measurements using a hot emissive probe and an ion sensitive probe. The sensor technology can be used to monitor plasma-based manufacturing systems, plasma-based energy generation systems, and as on-board plasma diagnostics in spacecraft including nanosatellites. [2013-0145]**

***Index Terms*— Electroless plating, high-density plasma diagnostics, high-frequency plasma diagnostics, MEMS Langmuir probes, through-substrate vias.**

I. Introduction

LANGMUIR probes (LPs) are used to estimate the electron temperature, electron density, and electric potential of a plasma. Due to their simplicity and low cost, LPs have been extensively used in characterizing a wide range of plasmas. Langmuir probes in the style of a wire protruding into the plasma have been the norm for plasma diagnostics since the inception of the technology in 1924 by Irving Langmuir. Though the use of microfabrication to produce plasma sensors is new and unconventional, the approaches hitherto followed the trend of 'sticking out' sensors [1]–[3]. However, the disadvantages of miniaturized protruding probes are numerous. One problem is that they can be more easily eroded by ions than macro versions because surface-to-volume ratio increases as the probe dimensions are scaled down; also, free-length structures develop higher stresses for a given load compared to identical structures fully supported. Therefore, miniaturized protruding LPs might not be an effective choice in demanding applications such as monitoring the plasma sheath formed during spacecraft reentry to the earth's atmosphere—of great importance to ensure the structural integrity, aerodynamic stability, and communication systems of the vehicle [4], [5].

Flush-mountable probes are an attractive alternative to circumvent the challenges faced by Langmuir probe miniaturization. Macro versions of flush-mounted Langmuir probe arrays have been reported to diagnose high-density plasmas [6]. Miniaturized flush-mountable Langmuir probe arrays (LPAs) can be used as 'sensorial skin' on spacecraft, tokamaks, or microfabrication plasma reactors to measure the plasma with high spatial resolution; these sensors can also be used as a scientific payload in a nanosatellite. With batch-microfabrication technology, a large number of probes can be built as a monolithic device, and many of these devices can be fabricated simultaneously [3], hence reducing the fabrication cost and increasing device reliability through redundancy. In addition, the benefits posed by these devices include deepening our understanding of plasma physics. For example, multiplexed MEMS LPs that are flush-mounted on a 3-D 'tip' or 'holder' can simultaneously capture fine details of plasma events in all axes without the need for reorientation. Also, different sensory configurations, e.g. single, double, triple probe devices, etc., can easily be implemented in a single die and thereby pave the way for their individual data acquisition strengths to be harnessed at the same time.

We report the design, microfabrication, and characterization of batch-fabricated flush-mounted MEMS LPAs for high-density plasma diagnostics, within HF to S bandwidth. Section II of the paper describes the design and fabrication

Manuscript received May 7, 2013; accepted February 11, 2014. Date of publication March 6, 2014; date of current version September 29, 2014. This work was supported by the U.S. National Aeronautics and Space Administration under Award NNC08CA58C. Subject Editor H. Fujita.

E. F. C. Chimamkpam was with the Massachusetts Institute of Technology, Cambridge, MA 02139 USA. He is now with the University of Cambridge, Cambridge CB2 1TN, U.K. (e-mail: emfrach@mit.edu).

E. S. Field was with the Massachusetts Institute of Technology, Cambridge, MA 02139 USA. She is now with Sandia National Laboratories, Albuquerque, NM 87123 USA (e-mail: efield@alum.mit.edu).

A. I. Akinwande and L. F. Velásquez-García are with the Massachusetts Institute of Technology, Cambridge, MA 02139 USA (e-mail: akinwand@mtl.mit.edu; lfvelasq@mit.edu).

Color versions of one or more of the figures in this paper are available online at http://ieeexplore.ieee.org.

Digital Object Identifier 10.1109/JMEMS.2014.2306631

of the MEMS LPAs. Section III describes the measurement circuits for the MEMS probes, and reports the characterization of the apparatus, i.e., the integrated electronics, fixtures, and MEMs chip. Section IV reports the testing of the sensor in a high-density helicon plasma source. Section V summarizes the work and suggests several directions for future research.

II. Microfabricated Langmuir Probe Arrays

A. Design Considerations

Our multiplexed plasma sensor is an array of individually addressable electrically conductive posts, embedded into a dielectric substrate; the spacing between the probes must be at least 3 times the plasma Debye length to avoid interference between adjacent probes [7]. The process flow to batch-fabricate the flush-mountable MEMS LPAs was chosen after evaluating the microfabrication technologies available to us. We explored Pyrex, alumina, and chemical vapor deposited silicon carbide (CVD SiC) as dielectric substrates, and we used nickel and gold to metallize the through-holes, i.e., vias, patterned on the dielectric substrates. Sensors made on Pyrex alone represent an advance in the state-of-the-art because, to the best of our knowledge, the only reported MEMS Langmuir probes utilize polymer insulators [1]–[3] that have a visibly lower melting temperature and are less resilient to sputtering and radiation damage; Pyrex is also inexpensive, widely available, and relatively simple to pattern due to the maturity of the fabrication technology used in microfluidics. However, for more stringent applications, silicon carbide- and alumina-based LPs would be a better choice because of their much higher thermal conductivity ($\geq$30 W/mK at 20 °C) and melting temperature ($\geq$2000 K).

We chose gold and nickel to metallize the vias because they have excellent corrosion resistance, thermal conductivity, and electrical conductivity, and because there are mature batch-microfabrication processes that can selectively deposit these materials onto vias. Gold and nickel can be deposited by an electroless plating method with deposition rates up to 25 μm/hr, which is sufficient to fill-in the largest vias we included in our design. However, nickel electroless plating chemicals are much cheaper and more readily accessible than those of gold.

We considered deep reactive-ion etching (DRIE), ultrasonic drilling, and laser drilling for patterning the vias. Even though DRIE can produce vias with aspect ratios as high as 1:25, the DRIE-patterned silicon vias would need to be coated with conformal dielectric films to meet the requirements of a dielectric substrate. However, this approach could create capacitive coupling problems between the probes if the coating is not thick enough. In addition, the devices could have reliability problems because the plasma could sputter the coating and short the probes. We concluded that ultrasonic drilling was the lowest-risk approach because it is a mature process for many materials including Pyrex, alumina, and CVD SiC. In addition, ultrasonic drilling has higher throughput compared to laser machining because it is done in parallel (i.e., all the holes of a substrate can be patterned at the same time) and the process provides the option for vias with tapered sidewalls in Pyrex. Moreover, ultrasonic drilling produces cleaner, more uniform holes compared to laser drilling, and it is capable of producing holes in dielectric substrates yielding diameters as small as 100 μm and an aspect ratio of 1:5. Ultrasonic-drilled vias have micron-sized sidewall roughness [8] that would help anchor the metallized probes to the substrate.

We started our investigations with Pyrex substrates because tapered holes (up to 30° sidewall inclination) can be ultrasonically drilled in Pyrex. We first preferred tapered sidewalls because they provide a measure of horizontal surface area of the sidewalls, which, we speculated, would help fill-in the vias with metal; however, our fabrication results demonstrate that holes with straight sidewalls are readily filled without voids, and in general, probe arrays with straight vias have higher probe density than probe arrays with tapered vias.

B. Fabrication

The key challenge to the fabrication of our plasma sensors is the metallization of vias to yield mechanically strong, non-protruding probes that are pore-free and with tip diameters close to the diameters of the vias. We successfully achieved this by the electroless plating method, i.e., an autocatalytic process that involves the presence of a chemical reducing agent in solution to reduce metallic ions to the metal state [9], [10]. Electroless plating does not require external electrical power; instead, a metal salt and a reducing agent in aqueous solution supply the metal and the electrons, respectively, when heated up.

A schematic of the fabrication process flow of our MEMS LPAs is shown in Fig. 1. The fabrication process of the MEMS LPAs began with ultrasonic drilling of vias arrays into 100 mm-diameter 0.38 mm-thick CVD SiC wafers (electrical resistivity $> 10^6$ Ω.cm), 50.4 mm-square 0.5 mm-thick alumina wafers, and 100 mm-diameter 0.5 mm-thick Pyrex (Corning 7740) wafers (Valley Design Corporation, Shirley MA). The size of each die was 10 mm $\times$ 10 mm, and each die contained an array of 2 $\times$ 2, 4 $\times$ 4, or 5 $\times$ 5 vias, with spacing between adjacent vias of 4, 2, and 1.6 mm, respectively. Straight-walled vias were drilled into the CVD SiC and alumina wafers, while both straight-walled and 30° tapered-walled vias were drilled into the Pyrex wafers (the taper of the vias was consistent across each die). The ultrasonic drilling of the substrates was outsourced to the company Bullen Ultrasonics (Eaton, OH). The plasma side of the vias has diameters in the range of 250 μm for alumina, 300 μm for CVD SiC, and 100–350 μm for Pyrex; we measured the diameter of the vias across multiple dies and typically found about 4 μm variation from average values across each array. The fabrication of the microprobes continued by coating the substrates with an airbrushed photoresist film, followed by sawing of the wafers into dies; a 280 μm-thick glass blade was used for the cutting of alumina and CVD SiC substrates while a 240 μm-thick glass blade was used for the cutting of the Pyrex wafers. After die-sawing, the protective photoresist coating was removed from the dies using a 3:1 mix of sulfuric acid and hydrogen peroxide; the dies were then rinsed with deionized water and dried using a nitrogen gun. The vias

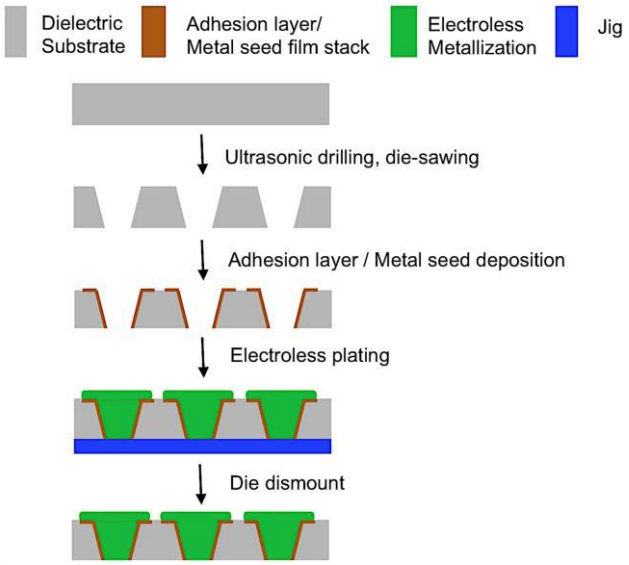

Fig. 1. Process flow to fabricate flush-mountable arrays of MEMS Langmuir probes.

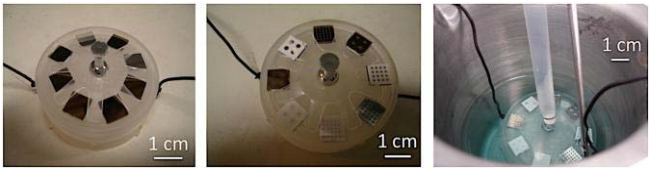

Fig. 2. Bare silicon dies used to prevent excessive plating on the frontside (left), chips mounted on top of the silicon dies (center), and a batch of dies during electroless plating (right).

were then coated with a 25 nm Ti/250 nm Au sputtered film stack using a shadow mask; the coating was applied on the backside of the dies, that is, the side for electrical connection that is unexposed to the plasma environment. After deposition of the gold seed layer on the backside of the dies, the vias were plated. We explored both electroless nickel and gold plating but we eventually down-selected nickel electroless plating due to its lower cost and equal performance in filling-in the vias compared to gold electroless plating. We used a plastic fixture to mount and secure each die face up on top of a blank piece of silicon to prevent excess nickel from being plated onto the frontside (i.e., the side for exposure to the plasma environment), minimize protrusion, and promote unidirectional filling. Our fixture allowed for eight dies to be processed at the same time. The fixture was then immersed in an electroplating bath inside a quarter-size container on top of a hot plate with magnetic stirrer; a thermocouple was used to monitor the temperature of the bath. Selected pictures of the plating process are shown in Fig. 2.

1) Tapered vs. Untapered Vias: One of the major concerns we had in the fabrication of the devices was the filling-in of the vias; we speculated that tapered vias were better than straight vias because they have sidewalls in the line of sight of the metal seed deposition. We were successful at fabricating devices using Pyrex substrates with tapered vias (Fig. 3, left); however, we realized that metallized tapered vias required substantially longer plating times to fully fill them in, and the

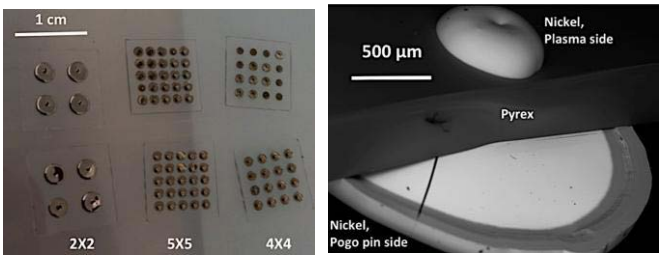

Fig. 3. Arrays of MEMS Langmuir probes made on Pyrex substrates with tapered vias (left), and cross section of one of the probes (right).

metallization process yielded probes with very large backside tip diameters (Fig. 3, right), limiting the array packing density. We also found that in some cases the metallization of a tapered via had a central hole that extended from the plasma side of the probe to the back of the probe. From our experiments we concluded that the metallization of straight vias yielded much better results than that of tapered vias in terms of closeness of the diameter of the metallization to the via diameter and the absence of voids in the metallization.

2) Tuning of Electroless Nickel Plating: We used electroless nickel plating solutions from Uyemura, Inc. (Ontario, CA) and Caswell, Inc. (Lyons, NY) for filling-in the vias. The Uyemura product was supplied in a ready-to-use-form (BEL-801), while the Caswell kit included nickel sulfate as the nickel source (i.e., Part A) and a reducing agent composed of sodium hypophosphite and ammonium hydroxide (i.e., Part B), which are combined with deionized water in the volume ratio of 1:3:16 of Part A, Part B, and deionized water, respectively, to form the plating solution. The two plating solutions yielded vias metallization with a different mix of strengths and weaknesses. On the one hand, the plating rate of the Uyemura's solution is about four times slower than that of the Caswell's; on the other hand, Uyemura's plating solution generates void-free metallization with flat and uniformly defined edges that match each via dimension and geometry and that firmly attach to the gold seed layer. We found that by using Uyemura's solution first, we obtained good adhesion of the metallization to the chip (die) and a well-defined nickel build-up from the seed layer that was uniform across the whole chip; we subsequently transferred the chips to Caswell's plating solution for completion of the vias metallization.

Proper temperature and stirring is required to fabricate zero-void probes; without them, the growth of the nickel layer inside the vias occurs at a much slower rate than at the surface because the reaction becomes supply-limited there. The nickel atoms spent in metallizing the via are only replenished by the flow of the solution in-and-out of the vias due to currents induced by the applied heat; the flowrate and the time allowed for the entire process determines whether the via is completely filled and devoid of holes. Fast deposition rates without any stirring of the solution leads to the formation of microprobes with holes. By increasing the rate of circulation due to stirring and process time, the process is no longer supply-limited and therefore, enough nickel is available for promoting the growth within the via. In our experiments, optimal enhancement of the vias filling-in rate was achieved by stirring of the

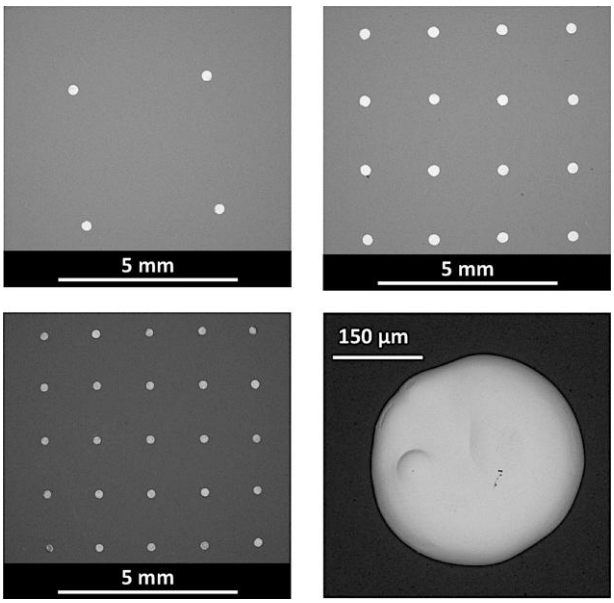

Fig. 4. SEM images of MEMS LPAs using substrates with untapered vias: (top left) 2×2 array made on a CVD SiC substrate with an average probe diameter of 295.0 ± 2.4 μm; (top right) 4×4 array made on a CVD SiC substrate with an average probe diameter of 314.5 ± 6.7 μm; (bottom left) 5×5 array made on an alumina substrate with an average probe diameter of 237.6 ± 7.0 μm; (bottom right) close-up of a single Langmuir probe with 304.6 μm tip diameter.

Uyemura's solution at 250 RPM and keeping the plating temperature at 65 °C, and by stirring of the Caswell's solution at 60–90 RPM while elevating the plating temperature to 113 °C. Fig. 4 shows SEMs of planar MEMS LPAs with as many as 25 probes (probe density as large as 39 probes/cm^2) using dielectric substrates with untapered vias and the electroless plating process we optimized. We obtained analogous results using Pyrex, alumina, and CVD SiC substrates.

III. Apparatus

A. Description

Measurement of high-density plasma events requires the use of fast sensors that can work at such frequency. Appropriate connectors, transmission lines, filters, and impedance matching are critical for passing along the signal from the probe to an observation system with a corresponding bandwidth. Our apparatus is composed of the MEMS LPA chip, a network of the probe electronics, signal transmission lines, feedthrough shaft, shielding box for the electronics, SMA connectors, flanges for vacuum seal, and electrical feedthroughs; our apparatus is capable of measuring plasma events at frequencies as high as 3 GHz.

Estimating the plasma sheath impedance at floating potential is advantageous for designing the circuit; when the plasma sheath impedance is matched with the input impedance of the probe, maximum signal is transmitted from the plasma to the probe and this enhances the accuracy of measured plasma characteristics. Assuming a probe of radius of 125 μm, the plasma sheath impedance at floating potential would range from $\sim 10^5$ to 10^6 Ω for an argon plasma with electron density $n_e = 10^{17}$ m^{-3} at electron temperatures in the range of 0.01–20 eV; this impedance drops down by 1-to-2 orders of magnitude for $n_e = 10^{18}$ to 10^{19} m^{-3}. The plasma sheath capacitance at floating potential for these ranges of densities and electron temperatures corresponds to $\sim$0.07–20 pF. The plasma sheath resistance at floating potential, i.e., R_s, and the plasma sheath capacitance at floating potential, i.e., C_s, were estimated according to the equations

$$R_s = \frac{k_B T_e}{n_e e^2 A} \sqrt{\frac{2\pi m_i}{k_B T_e}} \tag{1}$$

$$C_s(pF) = \alpha \times 1.49 \times 10^{-3} A\left(cm^2\right) \sqrt{\frac{n_e\left(cm^{-3}\right)}{K T_e\,(eV)}} \tag{2}$$

where n_e and T_e are the electron density and temperature, respectively, m_i is the ion mass, A is the probe area, and α is a constant (unity at floating potential) [11], [12].

We implemented a high-pass filter with a cutoff frequency of $\sim$2 MHz using a 0.1 pF capacitor and a 1 MΩ resistor; the time scale of 0.1 μs is adequate for rapid response to plasma fluctuations. The impedance is well matched with the estimated plasma sheath impedance, and the value of the resistor is also large enough (i.e., greater than $T_e/J_{e,sat}$, where $J_{e,sat}$ is the saturation current density) to measure the plasma potential. Since the plasma sheath resistance is less than or within range of the input impedance of the probe, a single probe from the MEMS LPA that self-biases to the floating potential would act as a floating-voltage probe.

The high-pass filter is subsequently networked to a voltage feedback preamplification circuit (THS4303 EVM, Texas Instruments Inc., Dallas, TX) that has a typical stable gain of 20 dB up to 1 GHz and 7 dB at 3 GHz. The plasma frequency for an electron density of 10^{17} m^{-3} is approximately 2.85 GHz, falling within the bandwidth of the circuit. We characterized our sensor system at MIT's Dynamics of Ionic Implantation and Sputtering on Surfaces (DIONISOS) helicon plasma source [13], where the helicon RF plasma discharges are driven at a frequency of 13.56 MHz and therefore, we expected our probe to be able to pick up signals at this fundamental frequency and any plasma harmonics. The active high-pass filter circuit is positioned very close to the probes in order to maximize signal preamplification before losses due to transmission to the read-out system occur.

Electromagnetic noise could substantially decrease the signal-to-noise ratio of our measurements. Therefore, it was essential to shield the electronics of our apparatus with a Faraday cage. We fabricated a shielding box consisting of a 85 cm (L) $\times$ 70 cm (W) $\times$ 2.5 cm (H) outer box made of aluminum for protection of probes' active high-pass filter circuit from plasma, and an inner box made of garolite (fiberglass) for heat shielding of the circuitry; the fiberglass box eliminates the need for cooling the electronics using forced-in pressurized air [2]. The outer aluminum box is attached to the long feedthrough and short probe shafts through threaded connections.

Instead of using vacuum epoxy to seal the feedthrough shaft, we used a 2.75" CF cross connected to the 1.2 m shaft via an interfacing Swagelok connector; this assembly allows for

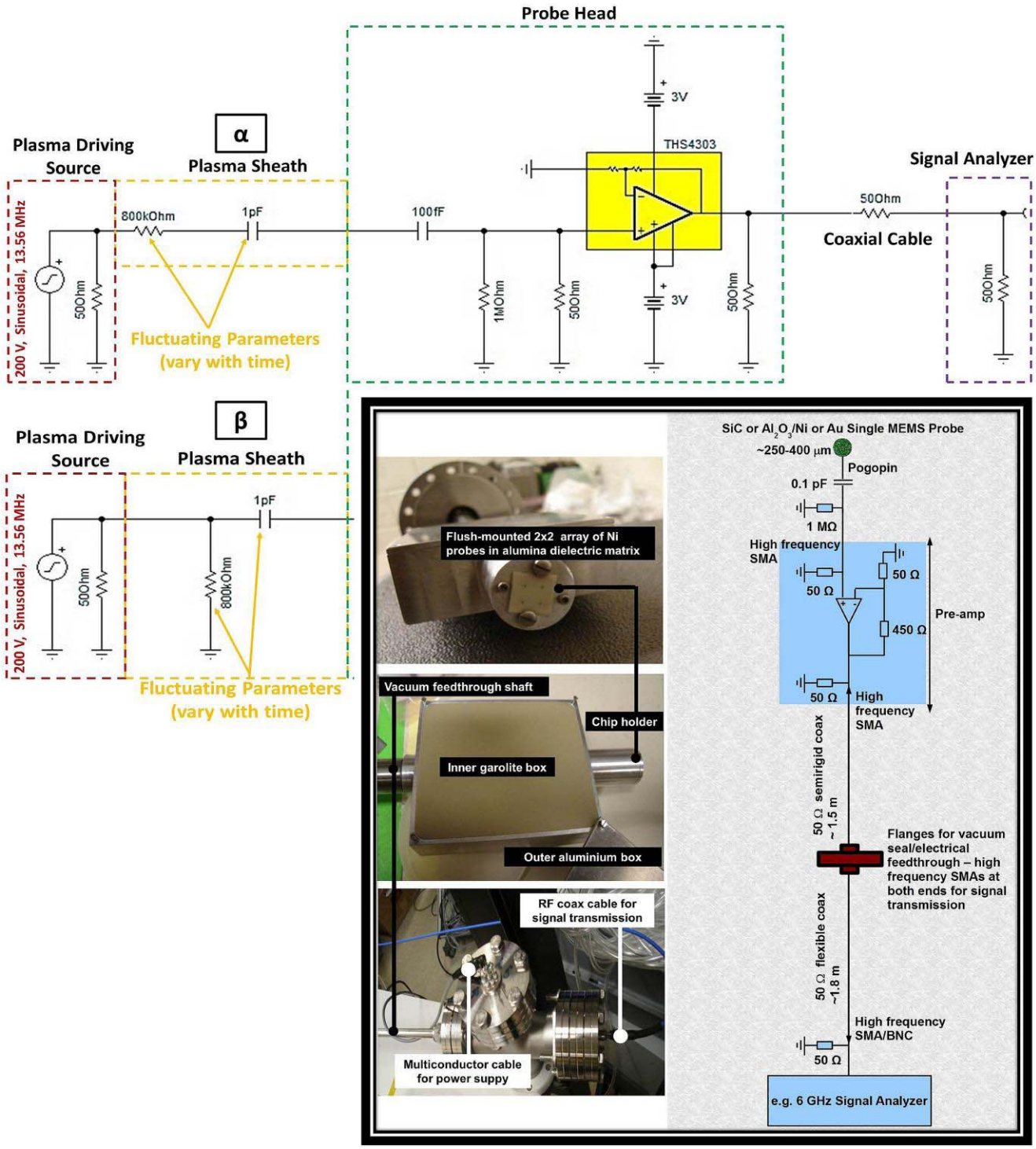

Fig. 5. Top - Circuit schematic where the coupled plasma sheath could take on alpha or beta form with *values* of capacitance and resistance varying over time, *in addition to switching of positions by the capacitor and resistor*. Bottom - Pictures of the apparatus (left) and illustration of the networked parts (right).

separate electrical feedthroughs (i) to supply DC voltage to the operational amplifier and to the probes (when needed), and (ii) to transmit the pre-amplified output signal to the observation system (oscilloscope or signal analyzer) via high-frequency SMA connectors. A 1.5 m 50 Ω impedance semi-rigid coax cable (Microcoax, Inc., Pottstown, PA) was used to cover the distance between the preamp and SMA CF flange seal. At the output of the op-amp circuit the impedance is 50 Ω, which we matched with the 50-Ω impedance of the transmission line coax to reduce signal losses and noise during transmission. For the power supply lines to the preamp circuit, a multi-conductor shielded cable was used and connected to a multi-pin electrical feedthrough. Fig. 5 shows the apparatus and a schematic of the circuit.

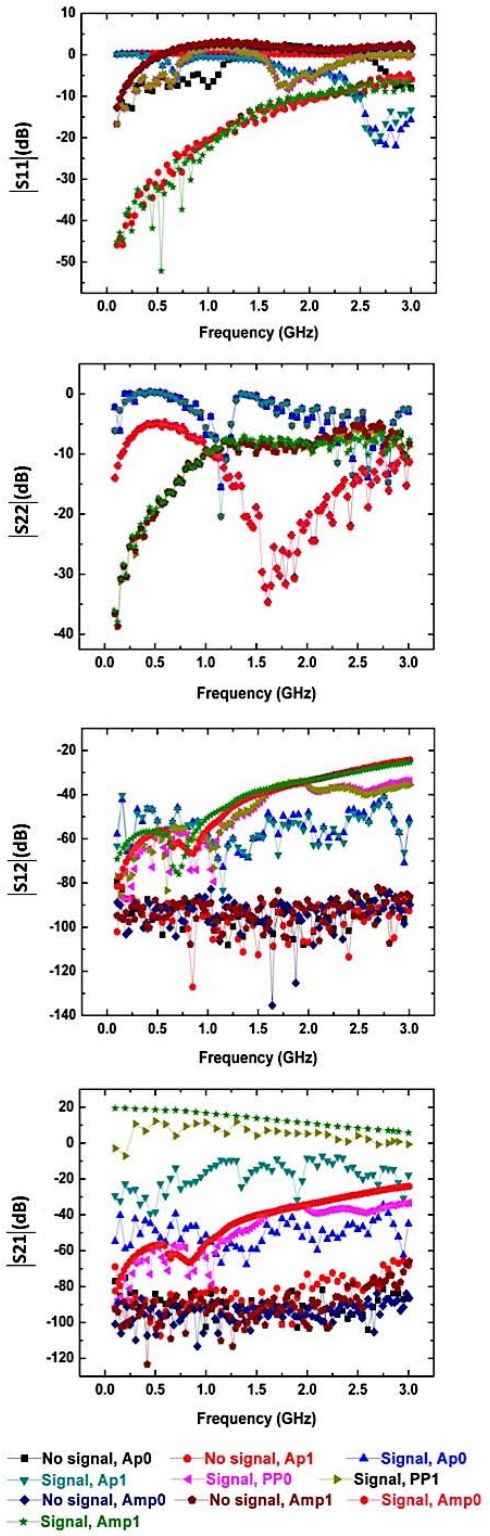

Fig. 6. S-parameters of apparatus (from top to bottom): S11, S22, S12, and S21 parameters at on (1) and off (0) states. Ap = apparatus; PP = pogo pin and amplifier only; Amp = amplifier only.

B. Apparatus Characteristics

The apparatus was characterized using a microwave ranged Function Generator/Oscilloscope, and an HP8510C Network Analyzer (Agilent Technologies, Inc. Santa Clara CA) was used for the S-parameters. Signals were fed through the apparatus at on and off states of the pre-amp circuit. Signal transmission without significant loss was obtained from the op-amp output (50 Ω) in the shielding box through the 50 Ω semi rigid coax (length of cable ∼1.5 m) passed along the feedthrough shaft to the vacuum side of a double-ended SMA CF flanged instrumentation feedthrough (50 Ω impedance), with a flexible coax (length of cable ∼1.8 m) connected to the air-side and down to a readout analyzer with 50 Ω impedance. This lossless signal transmission due to the networked matching impedances was confirmed by the S22 parameter (Fig. 6).

The pogo pin alone acting as an electrical connector of our surface-mounted probe has irregular RF features that are most obvious at the VHF and UHF bands when compared with the RF features of the op-amp (Figs. 6 and 7); this could be a result of the spring in the pogo pin, contour of the pogo pin socket, and/or contact between the pogo pin and its socket. However, without a spring-loaded connector such as the pogo pin, loss of contact between the surface-mounted probe and the electrical components can easily result; also, given the minimum probe separation in our devices (1.6 mm), one could readily assemble a monolithic array of commercially available pogo pins that interfaces with the probe array in the chip. One possibility to circumvent the need for pogo pin connectors would entail connecting a coax cable to each probe; this could be done by soldering a coax cable to the back of each probe, or by placing the coax cables inside the vias before the plating step.

Between the pogo pin and the input of the op-amp there is a high-pass filter that acts as a voltage divider circuit with a 50-Ω load. From Figs. 6 and 7, we can see the gains of the apparatus across various frequencies. The increase in gain from HF to S band is due to the decrease in the reactance of the capacitor at higher frequencies, which forms part of the voltage divider circuit. This frequency response trend is accounted for by the input impedance of our apparatus, which can accommodate up to 1 MΩ-level plasma sheath impedance. The results obtained from measurements of the apparatus using a function generator and oscilloscope strongly corroborate the S21 parameter obtained from the network analyzer when a signal is fed through the apparatus, at on and off states of the pre-amp circuit. The peaks in the curves are attributed to the contributions from the pogo pin. The experimental gains across the frequency ranges are reproducible at different input voltages (Fig. 7) and become therefore the characteristics of the apparatus as would be deployed into a plasma chamber. The averaged ratio of experimental gain to the predicted gain for the wide bandwidth (HF-S band) is 96.3%, i.e., the performance of the apparatus is close to the ideal case.

Repeatable characterization of the full apparatus over the relevant range of frequencies is important for obtaining reliable measurements of the plasma; without this characterization we would need to assume that all signal behavior comes from the plasma itself, which would result in erroneous estimation of the plasma parameters. Earlier work by Stilman et al [2] did attempt characterization of their MEMS LP but not of their entire apparatus. Furthermore, our S21 parameters when a signal is fed through the apparatus at an off state of the pre-amp indicate a gain akin to that reported by the authors using same THS4303 amplifier, which we consider as the

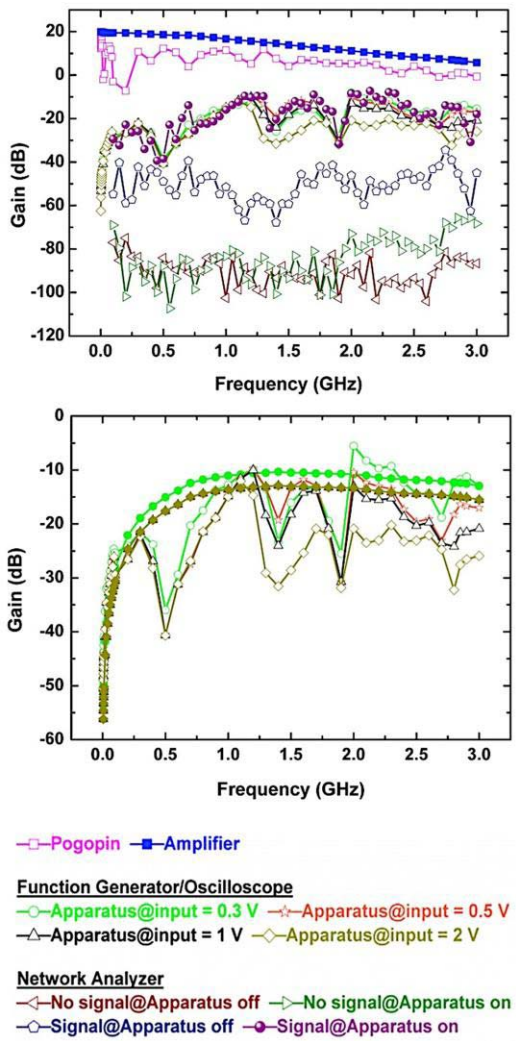

Fig. 7. Characteristics of apparatus: (Top) Comparison of data obtained from using a network analyzer and a function generator/oscilloscope (linear plot). S21 parameter corroborates gain from function generator/oscilloscope. 'No signal' implies complete disconnection of signal source from apparatus. (Bottom) Comparison of experimental (open symbols) and theoretical gains (closed symbols) of the apparatus.

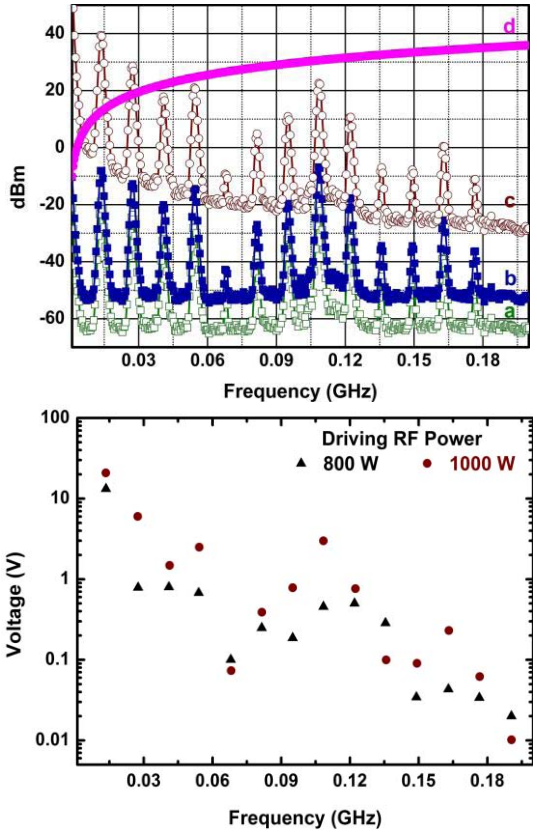

Fig. 8. Real-time plasma signature for measurements in the 0.01–0.2 GHz range. (Top): Spectrum (a) is the output on the signal analyzer. Spectrum (b) is the same output as spectrum (a) after taking the attenuations and gains into account. Spectrum (c) is the plasma characteristic, the actual voltage signal at the single 125 μm-radius probe after taking the signal through the potential divider filter circuit into account. Spectrum (d) is the model output that would have been observed on the signal analyzer if the probe had picked the RF source power at 1 kW, which is above the limit of the signal analyzer (+30 dBm). (Bottom): Magnitudes of the plasma harmonics at helicon source powers of 800 W.

background gain, that is less than the actual gain when a signal is fed through the apparatus at an on state of the pre-amp. The S11 and S12 parameters of our apparatus (Fig. 6) indicate no reflections when a signal is fed through the apparatus at on and off states of the pre-amp circuit.

IV. Real-Time Plasma Measurement

The plasma sensor system was tested in MIT's DION-ISOS [13], which can generate plasma with density up to 10^{19} m^{-3} using a helicon antenna driven by a 13.56 MHz radio-frequency (RF) source. Typical incident power can reach 3000 W, while the applied toroidal magnetic field can be as large as 0.1 T, and the argon pressure can go up to 2.7 Pa. The plasma sensor that we used for these measurements is comprised of a ~125 μm-radius single nickel probe part of a 2 × 2 LPA made on an alumina substrate that was flush-mounted onto its holder in the apparatus with the probe's backside attached to the pogo pin electrical connector. About 41 to 50 cm in length of the apparatus was mounted axially into the plasma chamber of ~83 cm in length and a spectrum analyzer (Agilent ESA E-Series) was used as a readout system. Our experiments were performed in argon at a pressure of 1.4–1.6 Pa, magnetic field of 25–41 mT, and RF source power of 800 to 1000 W. We estimate at 75–165 μm de Debye length of the plasma at the point of measurement ($T_e \sim 5$ eV, $n_e \sim 1 - 5 \times 10^{16}$ m^{-3}); therefore, an array of probes with ~225 μm probe separation or larger should be able to measure the plasma without a given probe perturbing the measurements conducted by the adjacent probes. The devices we made comply with this requirement as the densest LPAs we made have a probe separation of 1.6 mm.

Fig. 8 (top) shows the typical gain versus frequency data from our system when the helicon wave plasma is driven with 1000 W of RF power, a magnetic field of 41 mT, and Ar pressure of 1.6 Pa. We verified by running the same configuration multiple times that the data were repeatable. The single probe self-biases to the floating potential of the plasma on a timescale of 0.1 μs, which is adequate for observation of electrostatic fluctuations [14]–[16]. Plasma harmonics were

directly observed up to the 13th harmonic of the fundamental frequency (13.56 MHz); both odd and even harmonic components are apparent (Fig. 8 (top) and (bottom)). When there was no plasma in the chamber, no harmonics were detected. Fig. 7 shows that the apparatus does not exhibit characteristic resonances at frequencies less than 500 MHz (i.e., the frequency range where the harmonics were detected). Therefore, it is unlikely that the harmonics originated from the apparatus itself; instead, plasma-probe nonlinear interaction is apparently the source of these harmonics. For example, Dyson et al reported harmonics due to 'inherent plasma nonlinearity' even though they built a device to suppress the fundamental frequency and a few harmonics in order to determine the I-V characteristics [17]. According to the authors, the measured voltage $V(t)$ is a superposition of RF and DC voltages due to the plasma

$$V(t) = V_{DC} + V_{RF}(t) \tag{3}$$

with

$$V_{DC} = V_{applied} - V_{plasma} \tag{4}$$

where $V_{applied}$ is the voltage applied to the probe and V_{plasma} is the DC plasma potential. The RF voltage V_{RF} is the dominant contribution of a DC current enhancement parameter $I_0\left[\frac{eV_{RF}}{k_B T_e}\right]$, i.e.,

$$I_{DC} = I_0\left[\frac{eV_{RF}}{k_B T_e}\right] + I_{DC0(V_{DC})} \tag{5}$$

where $I_{DC0(V_{DC})}$ is the electron current in absence of RF, i.e.,

$$I_{DC0(V_{DC})} = I_e exp\left[{eV_{DC}}/{k_B T_e}\right] \tag{6}$$

From equations 3 to 6 it is clear that the plasma DC current and voltage depend on time varying functions; this leads to the question of distorted information due to targeted suppression of the inherent nonlinear nature of plasmas in order to apply DC theories.

Given the input impedance of our probe, which, as described in Section III, it is larger than or approximates the plasma sheath impedance, for plasma densities $\sim 10^{16}$–10^{19} m^{-3} at $T_e = 0.01$–20 eV, the RF potential is directly across the probe with almost no distortion in the measurement of the potential. Therefore, a spectrum of floating potential from our probe is a good estimate of the spectrum of plasma potential. The magnitude of the observed potential at the fundamental frequency is $\sim$21 V, which compares well with the plasma potential of 14–24 V typical at DIONISOS using a standard double Langmuir probe in a plasma generated at a source power of 1000 W, fill pressure of 1.15–1.5 Pa, and magnetic field of ca. 25–41 mT. It follows then that the range of plasma potential measured by the DIONISOS probe is due to the nonlinear behavior of plasmas; at best, the double Langmuir probe would fluctuate between signals at the fundamental frequency and close neighboring harmonics. The observed value of the plasma potential from our MEMS LP is two times lower than the value obtained using an emissive probe and an ion sensitive probe at a lower fill pressure of 0.2 Pa, with the same source power of 1000 W and magnetic field of 40 mT [18]; this was as expected because T_e, which is directly proportional to the plasma potential, is sensitive to pressure and decreases by a twofold when the argon fill pressure is increased 8 times [19], i.e., from 0.2 Pa in the experiments reported in Ochoukov et al in [18] to 1.6 Pa in our experiments. We conclude that the self-biasing probe successfully measured the plasma potential at DIONISOS because of its impedance that is greater than or within range of the sheath impedance.

The richness of the plasma spectra with higher-order harmonics suggests an asymmetrically driven RF discharge configuration, wherein the electrodes are unequal in area with at least one of the electrodes being floated [20]; the multi-harmonic signature is reduced as the asymmetry of a system is reduced [21]. Based on the magnitude of the fundamental harmonic, we consider the RF sheath in our experiments as collisional, i.e. ratio of plasma voltage to driving voltage $\sim$6.6% for source power of 800 W, and $\sim$9.3% for source power of 1000 W; these values are in agreement with the model for collisional RF capacitive sheath [20], [22].

V. Discussion

We demonstrated a novel MEMS Langmuir probe technology that is capable of measuring fast plasma fluctuations in high-density plasmas using a high-frequency technique in which the probe is measured at short time scales compared to the fluctuations of the plasma. In addition, we demonstrated that $V_{applied}$ is not crucial for deducing the plasma potential, and we also showed that there is agreement between our MEMS LP probe potential at the fundamental frequency and the plasma potentials obtained from a standard DC probe as well as from an emissive probe [18].

We propose a number of directions for extending the research on the technology. A first direction would entail taking advantage of the monolithic fabrication of a plurality of miniaturized Langmuir probes to implement multi-probe configurations to more efficiently measure the plasma properties; for example, double Langmuir probes can be implemented [23] and in this configuration voltage sweeping would be required. Also, triple Langmuir probes can be configured, which would allow faster sampling of the plasma because no voltage sweeping is required; other advantages of the triple Langmuir probe configuration over the double probe configuration are the feasibility to obtain spectral information of the plasma and the measurement of the plasma potential [24]. In addition, emissive probes [25] could be implemented using high temperature-compatible dielectric matrices such as alumina. All these probes can only be deployed in plasma conditions where the separation between adjacent probes is greater than at least three times the Debye length; otherwise, otherwise, cross-talking of the adjacent probes would occur. For example, if the probes were immersed in a plasma with electron temperature of 10 eV, the 5×5 arrays of probes we made would be limited to measure plasma densities of greater than or equal to 10^{16} m^{-3}, while the 4×4 and 2×2 arrays would be limited to measure plasma densities of greater than or equal to 10^{15} m^{-3}. Therefore, the denser the probe arrays, the less suitable they would be for use in low-density plasma diagnostics.

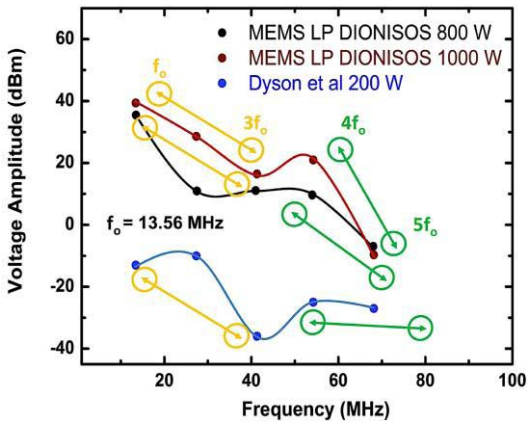

Fig. 9. Shapes of harmonic amplitudes derived for argon plasma excited at a fundamental frequency of 13.56 Hz. Consistent shape orientations for f_o to $3f_o$ at different plasma generating conditions and varying shape orientations for $4f_o$ to $5f_o$ at varied plasma generating conditions. The generating systems in all the cases are asymmetric.

Our probe system could also be used to observe peculiar plasma phenomena. For example, our devices should be able to observe electron phase-space holes, which are nonlinear plasma structures formed from strong current- or beam-driven turbulence that are responsible for the explosive release of magnetic energy in magnetospheric storms, solar flares, and laboratory plasmas [14], [26]. To observe these plasma fluctuations, fast microprobe systems working at high frequencies (at least up to plasma electron frequency with probe impedance greater than or within range of plasma sheath impedance) are indispensable [15], [16].

Finally, plasma harmonics should be further studied, as they may contain important information about the particular plasma produced and its generation scheme. For example, Fig. 9 suggests a common amplitude-frequency characteristic upon visualizing the relative amplitudes of the fundamental and first four harmonics (i.e. first five peaks) in Fig. 8 and those reported (irrespective of compensation) in [17]; it would be interesting to find out if the trend is real (can a plasma signature be derived from the harmonics?) and how general is this trend. It should also be investigated if portions of the amplitude vs. frequency curves (e.g., between the fundamental frequency, f_o and its harmonic at $3f_o$) are insensitive to compensation devices, structure of plasma chamber and/or operating parameters (magnetic field, RF power and gas fill pressure, etc.), while other portions of the curves (e.g., the harmonics at $4f_o$ and $5f_o$) reflect significant variations in the properties of the same type of plasma (e.g., T_e, RF power, etc.). Also, Stenzel et al observed a parametric instability in plasma due to periodic variation of sheath thickness [27]; the nonlinear behavior of this changing sheath thickness may be dependent on which gas molecules are used for the plasma generation and may manifest strongly on one of the harmonics. Definitive answers to these questions need further investigation.

ACKNOWLEDGMENT

The devices were fabricated at the MIT's Microsystems Technology Laboratories (MTL). The authors would like to thank D. Whytte, G. Wright, R. Sullivan, and J. Egedal from MIT's Plasma Science and Fusion Center (PSFC) for discussions and access to high-density plasma sources. They would also like to thank J. del Alamo, J. Scholvin, and T. Palacios from MIT's MTL for use of their RF stations and for discussions.

REFERENCES

[1] P. Pribyl, W. Gekelman, M. Nakamoto, E. Lawrence, F. Chiang, J. Stillman, *et al.*, "Debye size microprobes for electric field measurements in laboratory plasmas," *Rev. Sci. Instrum.*, vol. 77, no. 073504, pp. 1–8, Jul. 2006.

[2] J. A. Stillman, F. C. Chiang, P. Pribyl, W. Gekelman, M. Nakamoto, and J. W. Judy, "MEMS electric-field probes for laboratory plasmas," *J. Microelectromech. Syst.*, vol. 18, pp. 983–989, Oct. 2009.

[3] F. C. Chiang, P. Pribyl, W. Gekelman, B. Lefebvre, L.-J. Chen, and J. W. Judy, "Microfabricated flexible electrodes for multiaxis sensing in the large plasma device at UCLA," *IEEE Trans. Plasma Sci.*, vol. 39, no. 6, pp. 1507–1515, Jun. 2011.

[4] R. Lehnert, and B. Rosenbaum, "Plasma effects on Apollo re-entry communication," Nat. Aeronautics Space Admin., Goddard Space Flight Center, Greenbelt, MD, USA, Tech. Rep. NASA TN D-2732, 1965.

[5] W. L. Jones and A. E. Cross, "Electrostatic probe measurements of plasma surrounding three 25000 foot per second reentry flight experiments," NASA Langley Research Center, Washington, DC, USA, Tech. Rep. NASA SP-252, 1970.

[6] B. A. Carreras, V. E. Lynch, and B. LaBombard, "Structure and properties of the electrostatic fluctuations in the far scrape-off layer region of alcator C-Mod," *Phys. Plasmas*, vol. 8, no. 8, pp. 3702–3707, Aug. 2001.

[7] I. H. Hutchinson, *Principles of Plasma Diagnostics*, 2nd ed. Cambridge, U.K.: Cambridge Univ. Press, 2002.

[8] T. Diepold and E. Obermeier, "Smoothing of ultrasonically drilled holes in borosilicate glass by wet chemical etching," *J. Micromech. Microeng.*, vol. 6, no. 1, pp. 29–32, 1996.

[9] M. Schlesinger, "Electroless deposition of nickel," in *Modern Electroplating*, 5th ed. M. Schlesinger and M. Paunovic, Eds. Hoboken, NJ, USA: Wiley, 2010.

[10] H. O. Ali and I. R. A. Christie, "A review of electroless gold deposition processes," *Gold Bull.*, vol. 4, no. 17, pp. 118–127, 1984.

[11] J. C. Sprott, "Wide band electrostatic probes for use in tenuous plasmas," *Rev. Sci. Instrum.*, vol. 37, no. 7, pp. 897–900, Mar. 1966.

[12] P. J. Baum and J. Pollack, "Admittance probe measurements in the double inverse pinch device," *J. Appl. Phys.*, vol. 44, no. 1, pp. 163–167, Jan. 1973.

[13] (2014, Feb. 24). *Plasma-Surface Interactions Science Center—Dynamics of IONic Implantation and Sputtering On Surfaces (DIONISOS)* [Online]. Available: http://www.psisc.org/research/dynamics-ionic-implantation-and-sputtering-surfaces-dionisos

[14] W. Fox, M. Porkolab, J. Egedal, N. Katz, and A. Le, "Laboratory observation of electron phase-space holes during magnetic reconnection," *Phys. Rev. Lett.*, vol. 101, no. 255003, pp. 1–4, Dec. 2008.

[15] W. Fox, M. Porkolab, J. Egedal, N. Katz, and A. Le, "Observations of electron phase-space holes driven during magnetic reconnection in a laboratory plasma," *Phys. Plasmas*, vol. 19, no. 032118, pp. 1–12, Mar. 2012.

[16] W. Fox, M. Porkolab, J. Egedal, N. Katz, and A. Le, "Laboratory observations of electron energization and associated lower-hybrid and trivelpiece–gould wave turbulence during magnetic reconnection," *Phys. Plasmas*, vol. 17, no. 072303, pp. 1–18, Jul. 2010.

[17] A. Dyson, P. Bryant, and J. E. Allen, "Multiple harmonic compensation of Langmuir probes in RF discharges," *Meas. Sci. Technol.*, vol. 11, pp. 554–559, May 2000.

[18] A. R. Ochoukov, D. G. Whyte, B. Lipschultz, B. LaBombard, and S. Wukitch, "Interpretation and implementation of an ion sensitive probe as a plasma potential diagnostic," *Rev. Sci. Instrum.*, vol. 81, no. 10E111, pp. 1–3, Oct. 2010.

[19] T. P. Schneider, W. W. Dostalik, A. D. Springfield, and R. Kraft, "Langmuir probe studies of a helicon plasma system," *Plasma Sources Sci. Technol.*, vol. 8, no. 3, pp. 397–403, Aug. 1999.

[20] V. A. Godyak and R. B. Piejak, "Probe measurements of the space potential in a radio frequency discharge," *J. Appl. Phys.*, vol. 68, no. 7, pp. 3157–3162, Jun. 1990.

[21] M. N. A. Dewan, P. J. McNally, and P. A. F. Herbert, "Plasma modeling for a nonsymmetric capacitive discharge driven by a nonsinusoidal radio frequency current," *J. Appl. Phys.*, vol. 91, no. 9, pp. 5604–5613, May 2002.
[22] M. A. Liebermann, "Dynamics of a collisional, capacitive RF sheath," *IEEE Trans. Plasma Sci.*, vol. 17, no. 2, pp. 338–341, Apr. 1989.
[23] E. O. Johnson and L. Malter, "A floating double probe method for measurements in gas discharges," *Phys. Rev.*, vol. 80, no. 1, pp. 58–68, Oct. 1950.
[24] H. Lin, G. X. Li, R. D. Bengtson, Ch. P. Ritz, and H. Y. W. Tsui, "A comparison of Langmuir probe techniques for measuring temperature fluctuations," *Rev. Sci. Instrum.*, vol. 63, no. 10, pp. 4611–4613, Oct. 1992.
[25] E. Y. Wang, N. Hershkowitz, T. Intrator, and C. Forest, "Techniques for using emitting probes for potential measurement in RF plasmas," *Rev. Sci. Instrum.*, vol. 57, no. 10, pp. 2425–2431, Oct. 1986.
[26] B. Lefebvre, L.-J. Chen, W. Gekelman, P. Kintner, J. Pickett, P. Pribyl, *et al.*, "Laboratory measurements of electrostatic solitary structures generated by beam injection," *Phys. Rev. Lett.*, vol. 105, no. 11, pp. 115001-1–115001-4, 2010.
[27] R. Stenzel, H. C. Kim, and A. Y. Wong, "Parametric instability of the sheath-plasma resonance," *Radio Sci.*, vol. 10, no. 4, pp. 485–488, Apr. 1974.

Emmanuel F. C. Chimamkpam, photograph and biography not available at the time of publication.

Ella S. Field received the B.S. degree in mechanical engineering from the University of Minnesota, Minneapolis, in 2009 and an S.M. degree in mechanical engineering from Massachusetts Institute of Technology, Cambridge, in 2011. She is currently an engineer at Sandia National Laboratories developing optical coatings for the kilojoule class laser system coupled to the Z-Accelerator.

Akintunde Ibitayo (Tayo) Akinwande (S'81-519M'86-SM'04-F'08) is a Professor with the Department of Electrical Engineering and Computer Science, Massachusetts Institute of Technology, Cambridge. His research focuses on intelligent displays, large-area electronics, portable mass spectrometry, and field emission and field ionization devices.

Luis Fernando Velásquez-García (M'09-SM'10) is a Principal Scientist with the Microsystems Technology Laboratories, Massachusetts Institute of Technology, Cambridge. His research focuses on micro and nanoenabled multiplexed scaled-down systems that exploit high-electric field phenomena for space, energy, healthcare, manufacturing, and analytical applications.